

1-1-2021

Turkish perlite supported nickel oxide as the heterogeneous acid catalyst for a series of Claisen-Schmidt condensation reactions

SAKSHI KABRA MALPANI

DEEPTI GOYAL

STUTI KATARA

ASHU RANI

Follow this and additional works at: <https://journals.tubitak.gov.tr/chem>

 Part of the [Chemistry Commons](#)

Recommended Citation

MALPANI, SAKSHI KABRA; GOYAL, DEEPTI; KATARA, STUTI; and RANI, ASHU (2021) "Turkish perlite supported nickel oxide as the heterogeneous acid catalyst for a series of Claisen-Schmidt condensation reactions," *Turkish Journal of Chemistry*. Vol. 45: No. 4, Article 10. <https://doi.org/10.3906/kim-2010-42>
Available at: <https://journals.tubitak.gov.tr/chem/vol45/iss4/10>

This Article is brought to you for free and open access by TÜBİTAK Academic Journals. It has been accepted for inclusion in Turkish Journal of Chemistry by an authorized editor of TÜBİTAK Academic Journals. For more information, please contact academic.publications@tubitak.gov.tr.

Turkish perlite supported nickel oxide as the heterogeneous acid catalyst for a series of Claisen–Schmidt condensation reactions

Sakshi Kabra MALPANI¹ , Deepti GOYAL² , Stuti KATARA³ , Ashu RANI^{3*} ¹Department of Chemistry and Biochemistry, Faculty of Physical Science, Jyoti Nivas College Autonomous, Bengaluru, Karnataka, India²Department of Applied Chemistry, School of Vocational Studies & Applied Sciences, Gautam Buddha University, Greater Noida, UP, India³Department of Pure and Applied Chemistry, Faculty of Science, University of Kota, Kota, Rajasthan, India

Received: 20.10.2020 • Accepted/Published Online: 26.04.2021 • Final Version: 27.08.2021

Abstract: Potentially active and eco-friendly solid acid catalysts have been synthesized by loading different weight percentages (10, 15, and 50) of nickel oxide on thermally activated Turkish perlite through the deposition-precipitation method. Structural features of prepared catalysts were analyzed using BET surface area analysis, X-ray diffraction, scanning electron microscope (SEM), SEM-EDX, transmission electron microscopy (TEM), Fourier-transform infrared (FT-IR), pyridine adsorbed FT-IR, UV-Vis diffuse reflectance spectroscopy (DRS), and thermogravimetric analysis (TGA) techniques. Pyridine adsorbed FT-IR analysis confirmed the presence of the optimum amount of Bronsted acidic sites in a catalyst having 15 wt. % loading of nickel oxide, which was tested for catalyzing a series of Claisen–Schmidt condensation of cyclohexanone and aromatic aldehydes to produce good isolated yield (90%–93%) of 2,6-bis(substituted benzyldene)cyclohexanones, significantly used in anti-tumor and cytotoxic activities. The high catalytic efficiency of the chosen catalyst remains almost intact up to six reaction cycles. On higher wt. % loading of nickel oxide, crystallite size increases along with agglomeration of larger nickel oxide particles on catalyst surface resulting in pore blockage and poor catalytic activity. Loading of NiO on the surface of thermally activated Turkish perlite was confirmed by SEM-EDX analysis, and TEM observations show that the particle size of the preferred catalyst was less than 50 nm. Based on results drawn from XRD, FT-IR, pyridine adsorbed FT-IR, UV-Vis DRS studies, model structures were proposed for Turkish perlite and all prepared catalysts. During this work, the catalytic potential of the preferred catalyst was compared with other previously reported catalysts, and it showed appreciable results. The formed products were further confirmed by their melting point and ¹H-NMR analysis.

Key words: Turkish perlite, nickel oxide, solid acid catalyst, Claisen–Schmidt condensation, 2,6-bis(substituted benzyldene) cyclohexanones

1. Introduction

Acid catalysis is an important area of organic synthesis and vital industrial significance predominantly in the petrochemical, fine chemical, and pharmaceutical industries [1]. Many intrinsic drawbacks of the use of homogeneous acid catalysts have stimulated the research for recyclable strong solid acids to replace conventional, toxic, homogeneous acid catalysts. Heterogeneous catalysts such as phosphosulfonic acid, nano sulfated zirconia, and boric acid [2–4] are being utilized as a replacement of homogeneous acids in industrially important reactions. As a lucrative alternative to classical solid catalysts, the use of economical solid catalysts like activated fly ash precipitated silica catalyst, sulfated zirconia/fly ash, cerium triflate/fly ash, scandium triflate/fly ash, phosphomolybdic acid/fly ash, fly ash solid base catalyst [5–10], and other waste-derived catalysts [11–15] is gaining interest nowadays.

Perlite is a hydrated, pozzolanic, naturally occurring volcanic glass formed by the cooling of volcanic eruptions, estimating about 1.1 million metric tons production in Turkey [16]. It has a layered structure whose skeleton mainly comprises oxides of silicon, aluminium, potassium, and sodium, while oxides of titanium, calcium, magnesium, iron, and chemically combined water, etc. are present in small quantities [17]. Its particles are neutral, fluffy, non-toxic, can expand up to 20 times than their original volume on heating beyond 900 °C. Its particle size and specific surface area are 0.2–4 mm and 1.22 m²g⁻¹ respectively [18,19]. It is mainly used in producing construction materials, adsorption and removal of atmospheric pollutants, horticulture, etc. [20–22], while its application in heterogeneous catalysis is not much explored in past except only a few reports [23–30]. Turkey is the third worldwide leading producer of perlite and accounts for about

* Correspondence: ashu.uok@gmail.com

16% of its total production [14]. It is, thus, assumed that Turkish perlite, which has high silica and alumina composition might possess significant stable surface-active sites and can be converted into a potential heterogeneous acid catalyst for catalyzing industrially beneficial organic transformations. Nickel-based catalysts supported on different substrates like silica, alumina, zeolites have attracted research attention because of their potential applications in many important reactions such as hydrogenation, diesel steam reforming, ozonation of 2,4-dichlorophenoxyacetic acid, dry reforming of methane [31–34], etc. Particularly, supported nickel oxide catalysts have been utilized in numerous potential reactions such as hydrogen production, oxidative dehydrogenation, hydrogen peroxide decomposition, etc. [35–37], while fewer records are found for its application in condensation reactions [38]. Catalyst support is vital as it facilitates higher dispersion of nickel oxide and prevents its aggregation [39], which, in turn, enhances the efficiency of catalyst, and, thus, maximum conversion and yield % of desired products are achieved. With the increasing social interests over environmental degradation and future resources, it is of great importance for chemists to come up with new approaches that are less hazardous to human health and the environment. In this series, we have tried to explore stable surface-active sites of a novel silica-alumina enriched natural waste- Turkish perlite and its efficiency as catalyst support.

In the current work, a novel, efficient Turkish perlite supported nickel oxide catalyst (NPC-15) was prepared by loading nickel oxide on thermally activated Turkish perlite (TAP), and it successfully catalyzed a series of Claisen–Schmidt condensation reactions giving a higher isolated yield % of desired products, 2,6-bis(substituted benzylidene) cyclohexanones, used in anti-tumor, anti-cancer, and cytotoxic activities [40] and also serve as an important precursor for the synthesis of potentially bioactive pyrimidine derivatives [41, 42]. Table 1 summarizes some nickel catalysts supported on economical substrates already precedented in literature, utilized in different reactions including Turkish perlite supported nickel oxide catalyst (NPC-15) presented in this work. Our work is different and innovative in terms of sustainability and reusability of NPC-15 up to six consecutive reaction cycles, also the catalytic potential of NPC-15 was tested for a series of Claisen–Schmidt condensation reactions, which is quite an uncommon field of catalysis for supported nickel oxide catalysts. Use of less expensive support, recyclable catalyst, solvent-less reaction conditions, green methodology, ease of product purification are the key features of this protocol, and, thus, it may be considered as an efficient alternative to the existing, high-priced, less-effective procedures. This work is aimed to act as a stepping-stone for the prospective researchers into the rewarding field of utilization of waste materials like Turkish perlite as the catalyst support in the development of heterogeneous catalysts.

2. Experimental

2.1. Chemicals

Nickel nitrate, sodium hydroxide, nickel oxide, cyclohexanone, and aromatic aldehydes were purchased from Sigma Aldrich, Bengaluru, Karnataka, India. Turkish perlite was supplied by Indica Chem. Ind. Pvt. Ltd., Kotdwar, Uttarakhand, India.

Table 1. Various nickel catalysts supported on different, economical substrates.

Name of catalysts	Supports used	Chemicals used	Method used for catalyst synthesis	Catalytic applications
NiFA _k [37]	Fly ash	Ni(NO ₃) ₂ .6H ₂ O, CaO, urea	Microwave assisted solution combustion	H ₂ O ₂ decomposition
NiPCH [36]	Porous clay heterostructures	Ni(NO ₃) ₂ .6H ₂ O, oxalic acid	Evaporation	Oxidative dehydrogenation of ethane
Ni/SiO ₂ -RHA [43]	Rice husk ash	Ni(NO ₃) ₂ .6H ₂ O, aq. NH ₃	Ion exchange	-
Ni-10/AC [44]	Activated carbon	Ni(NO ₃) ₂ .6H ₂ O	Wet impregnation	Benzaldehyde hydrogenation
Ni/PF-B [26]	Perlite treated with Na ₂ CO ₃	Ni(NO ₃) ₂ .6H ₂ O and Mg(NO ₃) ₂ .6H ₂ O, solid anhydrous Na ₂ CO ₃	Co-precipitation followed by reduction	Sunflower oil hydrogenation
Nickel boride catalyst [45]	Hydrothermal modified perlite	NiCH ₃ (CO ₂) ₂ .4H ₂ O, NaBH ₄ , NaOH	Impregnation	Hydrogenation of nitrobenzene
NPC-15 [This study]	Turkish perlite	Ni(NO ₃) ₂ .6H ₂ O, 6 M NaOH solution	Deposition-precipitation	Series of Claisen-Schmidt condensation reactions

2.2. Catalyst synthesis

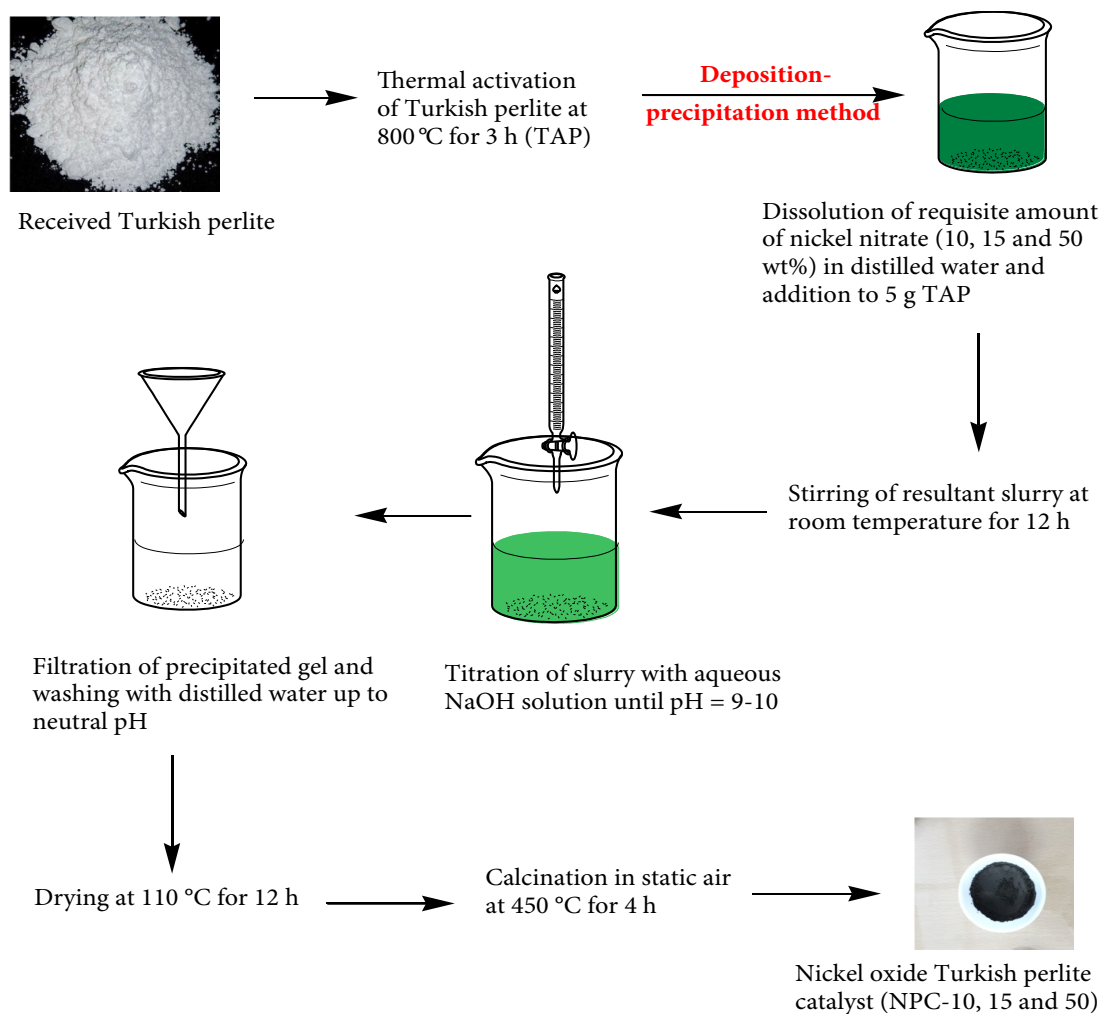
After being received, Turkish perlite was initially activated thermally at 800 °C for 3 h to remove moisture, carbon, and other impurities to form TAP (thermally activated perlite). All the catalysts investigated in this study (NPC-10, 15, and 50) were synthesized by loading 10, 15, and 50 wt.% nickel oxide on TAP by deposition-precipitation method, using NaOH as a basification agent. The required amounts (1.97 g for 10 wt. %, 2.95 g for 15 wt. %, 9.83 g for 50 wt. %) of precursor salt (nickel nitrate) in an aqueous solution phase were mixed with 5 g of TAP and agitated for 12 h at room temperature. Thus, obtained homogeneous mixture of metal salt and TAP was treated with 6 M NaOH solution until pH value becomes 9–10. Then, formed precipitated gel was filtered, washed several times up to neutral pH, dried at 110 °C for 12 h, and then calcined in static air at 450 °C for 4 h. The negative results of Dimethylglyoxime (DMG) tests confirm that no nickel ions leached off from the catalysts during their synthesis. The synthesis process of NPC catalyst is presented in Scheme 1.

2.3. Catalyst characterization

Structural and morphological features of all catalytic materials were analyzed by BET surface area analysis (Anton Paar India Pvt. Ltd., Gurgaon, Haryana, India), XRD (Bruker, Mumbai, Maharashtra, India), SEM, SEM-EDX JEOL India Pvt. Ltd. Mumbai, Maharashtra, India.), TEM (Hitachi High-Tech India Private Limited, Mumbai, Maharashtra, India), FT-IR, pyridine adsorbed FT-IR (Bruker, Mumbai, Maharashtra, India), UV-Vis DRS (Perkin Elmer (India) Pvt Ltd., New Delhi, India) and TGA (Mettler Toledo) techniques. ¹H NMR spectra of products were recorded on Bruker DRX300 spectrometer.

2.4. Catalyst evaluation

The condensation reactions (Scheme 2) catalyzed by NPC-10, 15, and 50 were performed in a liquid phase batch reactor equipped with 250 mL RBF (round bottom flask), magnetic stirrer, and spiral glass condenser, placed in a thermostat. In



Scheme 1. Synthesis of nickel oxide Turkish perlite catalyst.

this procedure, a mixture of cyclohexanone and aromatic aldehydes (molar ratio = 1:2) was placed in a RBF and mixed with the activated catalyst. The reaction mixture was stirred at different times and temperatures. Once the reaction is over, the catalyst was removed from the reaction mixture by simple filtration. Melting points of products were detected by using Melting Point System MP30, Mettler Toledo India Pvt. Ltd., Vasai, Maharashtra, India, melting apparatus.

$$\text{Isolated yield \% of 2,6-bis(substituted benzylidene)cyclohexanone obtained}$$

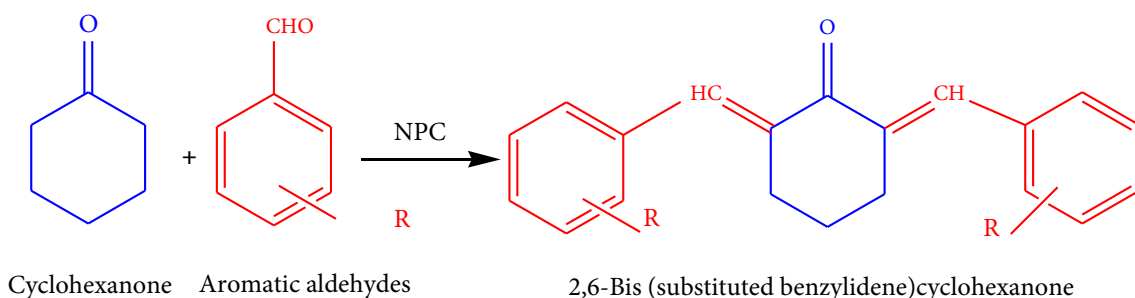
$$= 100 \times \frac{\text{g of 2,6-bis(substituted benzylidene)cyclohexanone obtained experimentally}}{\text{g of 2,6-bis(substituted benzylidene)cyclohexanone obtained theoretically}}$$

3. Results and discussion

3.1. Characterization of catalysts

Table 2 shows the surface properties of Turkish perlite and NPC-10, 15, and 50 catalysts with different nickel oxide loadings (10, 15, and 50 wt. %). The results indicate that when the nickel oxide loading increased from 10 to 15 wt. % in NPC catalyst, a decrease in the surface area was observed. Further increase in nickel oxide loading resulted in a significant decrease in surface area, which may be due to the blockage of pores of Turkish perlite by nickel oxide dispersion. Thus, from these results, it can be established that an increase in nickel oxide loading is responsible for the agglomeration of nickel oxide species to form bigger particles, and, thus, their diffusion decreases. These results are in good agreement with XRD results. Despite this, it was also observed that in NPC-10 and 15 the crystallite size remains unaltered, but, on further increase in nickel oxide loading, crystallite size also increased. The above discussion indicated that higher wt. % loading of nickel oxide does not provide sufficient active sites due to their agglomeration as inferred from increased crystallite size [46,47].

The XRD of Turkish perlite (Figure 1a) shows the existence of a hump between $2\theta = 10\text{--}15^\circ$ attenuated to amorphous silica [48]. However, in TAP, a small crystalline peak appears at $2\theta = 27.642^\circ$ (Figure 1b) which confirms the formation of quartz crystalline phase in the sample on heating [49] along with a broad hump at $2\theta = 22\text{--}23^\circ$ showing amorphous content of silica [50,51]. The absence of crystalline peaks in X-ray diffraction patterns of NPC-10 and 15 (Figures 2a and 2b) is due to the dispersion of nickel oxide particles on the Turkish perlite surface in the amorphous phase and tiny in size to give an XRD peak [52] in lower wt. % catalysts. While, in case of NPC-50 (Figure 2c), small peaks begin to appear at $2\theta = 37.26, 43.29, 62.88^\circ$ corresponding to Miller indices [003], [012] and a combination of the [104] and [110] reflections of nickel oxide, respectively [53], which are evident of formation of Ni-O phase in the sample. However, because of the weak, broad, and partially overlapping peaks, the crystallite size determination of the nickel oxide containing phase is difficult in NPC-50 [54].



Scheme 2. Condensation of cyclohexanone and aromatic aldehydes over NPC to give 2,6-bis(substituted benzylidene) cyclohexanone.

Table 2. BET specific surface area of samples.

Samples	BET specific surface area (m^2/g)
Turkish perlite	2.3
NPC-10	2.2
NPC-15	1.9
NPC-50	1.1

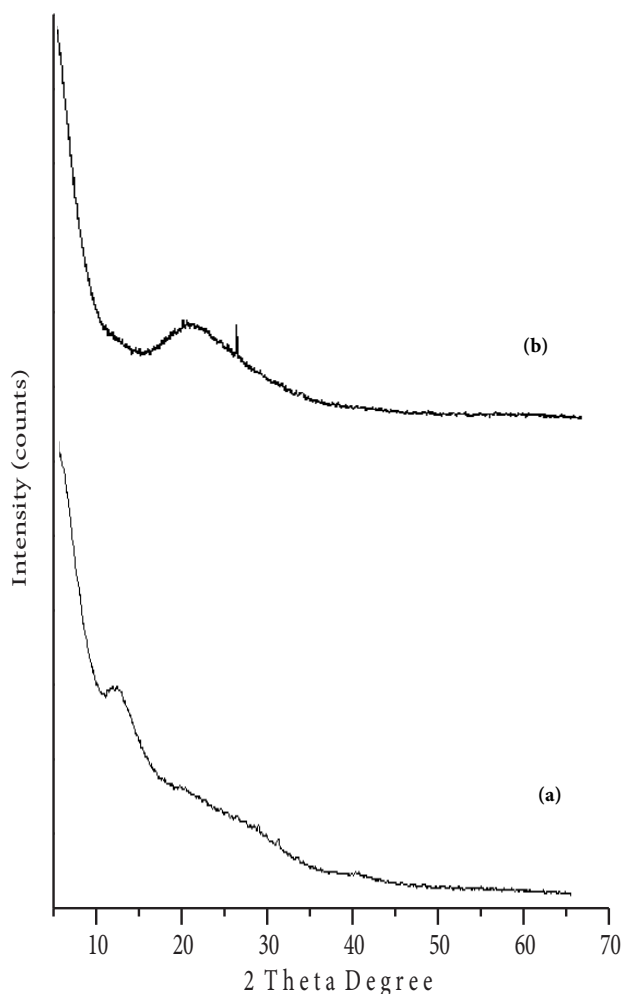


Figure 1. X-ray diffraction patterns of (a) Turkish perlite and (b) TAP.

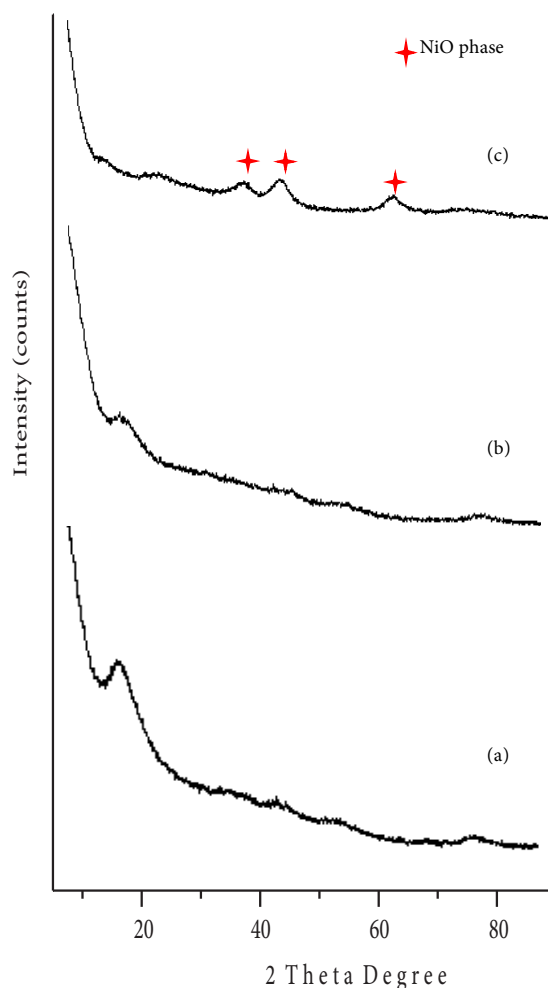


Figure 2. X-ray diffraction patterns of (a) NPC-10, (b) NPC-15 and (c) NPC-50.

SEM micrograph of Turkish perlite (Figure 3a) revealed randomly placed irregular shred particles with uneven edges, open pores also shown in other reports [55, 56]. SEM image of TAP (Figure 3b) is mainly fragmentary, glassy, and random [57], but the morphology is less irregular indicating removal of water at a high temperature, which leads to a reduction in porosity and also agglomeration of smaller particles. SEM images of NPC-10, 15, and 50 (Figures 3c, 3d, 3e) demonstrate the dispersion of shiny, fine nickel oxide particles on the surface of Turkish perlite. It was also found that the porosity of Turkish perlite particles was decreased on the loading of nickel oxide.

EDX analysis of Turkish perlite, NPC-10, 15, and 50 (Table 3) shows the presence of SiO_2 , Al_2O_3 , K_2O , Na_2O , and other minor metal oxides in the samples. However, the presence of nickel oxide in all NPC catalysts confirms its effective loading on the Turkish perlite surface.

A more realistic vision of irregular morphology, ragged shreds of Turkish perlite can be furnished by its TEM image (Figure 4a). The micrograph of NPC-15 (Figure 4b) shows fine dispersion of nickel oxide particles on the Turkish perlite surface. These results are in agreement with SEM images. TEM observations also show that the particle size of NPC-15 is less than 50 nm.

FT-IR spectrum of Turkish perlite is shown in Figure 5a. A broad band in the range between $3700\text{--}3000\text{ cm}^{-1}$ shows the presence of surficial hydroxyl groups ($-\text{Si}-\text{OH}$) with strong intermolecular hydrogen bonding and physisorbed water molecules [58,59]. The intensity and broadness of this band diminished in TAP (Figure 5b), which is due to the loss of water as a consequence of thermal activation. A peak at 1178 cm^{-1} , attenuated to the Si-O-Si asymmetric vibrational frequency, confirms the presence of silica skeleton in Turkish perlite. After thermal activation, this peak gets shifted to 1227 cm^{-1} ,

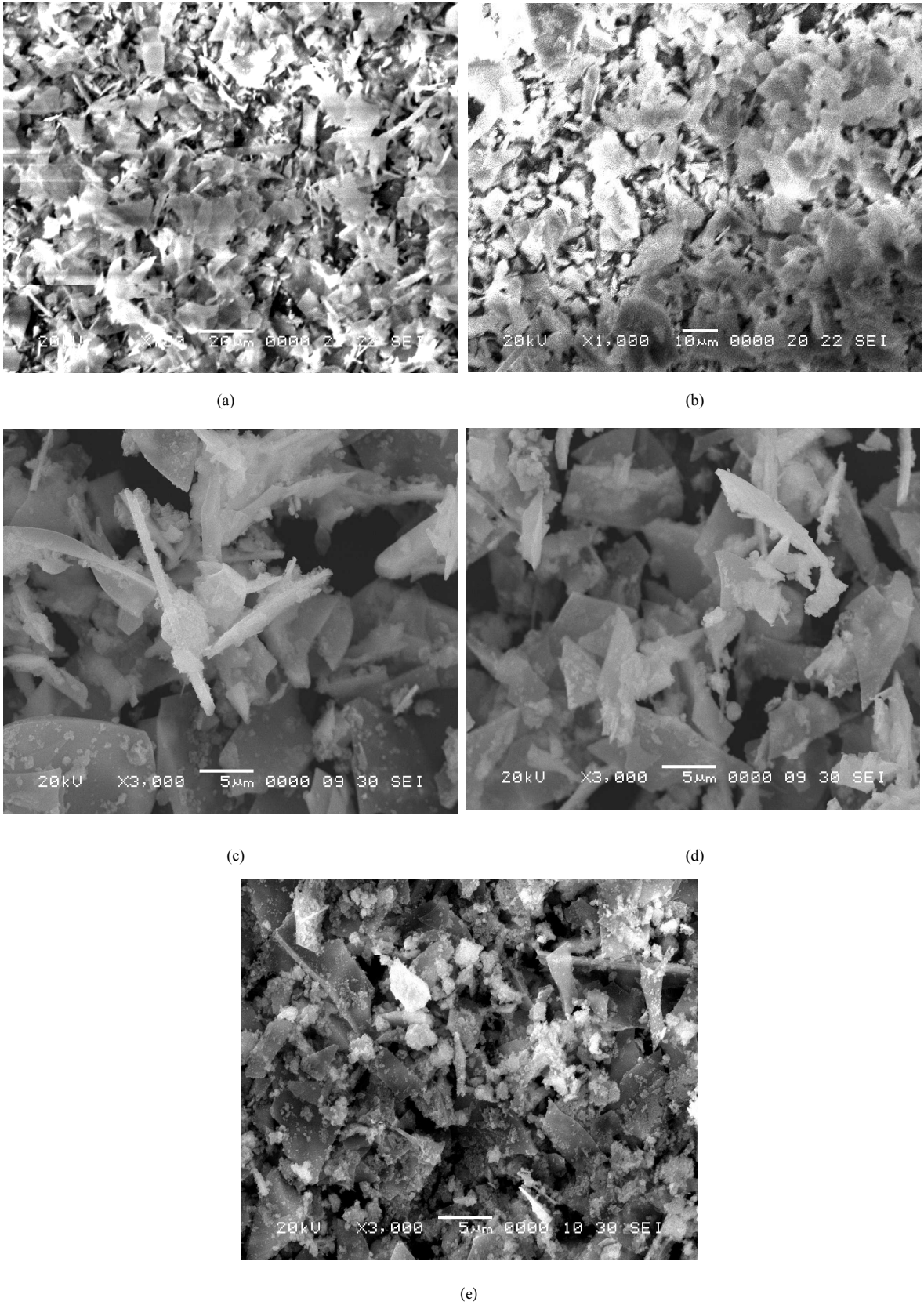
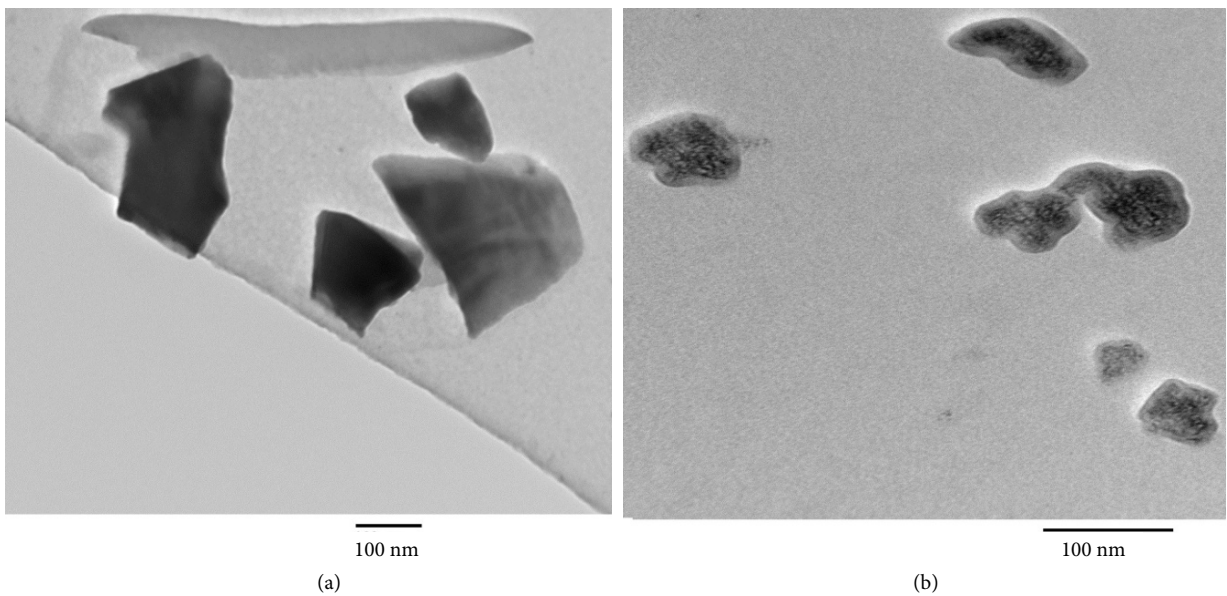
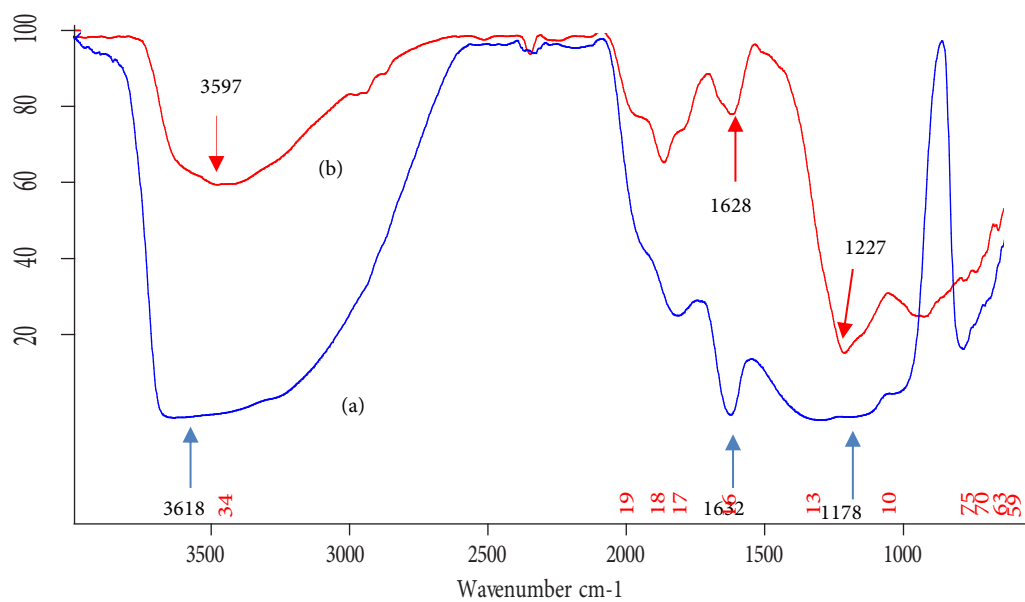


Figure 3. SEM micrographs of (a)Turkish perlite, (b) TAB, (c) NPC-10, (d) NPC-15 and (e) NPC-50.

Table 3. EDX analysis of Turkish perlite, NPC-10, NPC-15, and NPC-50.

Samples	SiO ₂ (wt%)	Al ₂ O ₃ (wt%)	K ₂ O (wt%)	Na ₂ O (wt%)	ZnO (wt%)	FeO (wt%)	NiO (wt%)	LOI
Turkish perlite	72.74	14.79	7.48	2.10	2.04	0.91	-	4.1
NPC-10	71.09	12.14	5.68	1.86	-	-	8.42	1.2
NPC-15	67.40	11.69	5.24	1.78	-	-	13.89	0.8
NPC-50	40.28	9.47	-	1.54	-	-	48.69	0.24

LOI- Loss on ignition

**Figure 4.** TEM micrographs of (a) Turkish perlite and (b) NPC-15.**Figure 5.** FT-IR spectra of (a) Turkish perlite and (b) TAP.

which is a common phenomenon in amorphous silica samples [60]. An intense peak around 1630 cm^{-1} in Turkish perlite, characteristic of bending mode ($\delta_{\text{O-H}}$) of water molecule [61,62] again highly decreased in TAP.

While loading nickel oxide on TAP, its surface gets activated by hydroxyl groups because aqueous NaOH was used as a basification agent during catalyst preparation. Consequently, the FT-IR spectra of NPC-10, 15, and 50 (Figure 6) show an increase in broadness and peak intensity of the band attributed to $-\text{OH}$ groups. A new band appeared around 1050 cm^{-1} can be assigned to $\equiv\text{Si-O-Ni}$ stretching vibration [63], which is normally observed in the range of $1100\text{--}1000\text{ cm}^{-1}$, but, here, it cannot be resolved because of its overlap with the absorbance of Si-O-Si stretching, appearing in the range of $1300\text{--}1000\text{ cm}^{-1}$. An absorption band due to surficial Si-O-Ni stretching vibration has appeared at 964 cm^{-1} [64]. It is also found that the intensity of the band was increased to some extent after increasing nickel oxide incorporation.

The FT-IR spectra of NPC-10, 15, and 50, obtained after pyridine adsorption in the range of $1550\text{--}1400\text{ cm}^{-1}$ are shown in Figure 7. The peak at 1538 cm^{-1} (Figure 7a) indicates the presence of few Bronsted acidic sites in NPC-10. In NPC-15 (Figure 7b), a peak and a broad band appearing at 1438 and 1540 cm^{-1} , respectively [65–67] show the existence of some Lewis and optimal Bronsted acidic sites for suitable catalytic activity. NPC-50 has the highest Lewis acidic sites corroborated by the appearance of intense peaks at 1438 and 1450 cm^{-1} (Figure 7c).

UV-Vis DRS is used to determine the state of nickel oxide incorporated into the Si-O-Si skeleton of TAP. During steps of synthesis, due to the calcination of catalysts at $450\text{ }^\circ\text{C}$ for 4 h, the presence of $\text{Ni}(\text{OH})_2$ can be declined. A broad band around 250 nm (Figure 8), which becomes more intense with an increase in weight percentage of nickel oxide loading suggests that Ni^{+2} ions are in an octahedral local environment [68].

The TGA and DSC curve of NPC-15 (Figure 9) comprises of two main regions having a major weight loss of about 8.96% up to $643.83\text{ }^\circ\text{C}$ and a minor one of approximately 0.82% weight loss at higher temperature along with an exothermic DSC peak. The weight loss in the first region could be due to the removal of bulk water, physisorbed water, and loosely bound hydroxyl groups [69], and decomposition of nickel salt (used as a precursor) [70]. The second region shows a minor weight loss, which may be due to the conversion of $\text{Ni}(\text{OH})_2$ into NiO .

3.2. Catalytic activity

The catalytic performance was preliminarily tested by Claisen–Schmidt condensation reaction of cyclohexanone and benzaldehyde to give 2,6-bis(benzylidene)cyclohexanone in a single step, one-pot reaction conditions. The reaction was carried out at $120\text{ }^\circ\text{C}$ for 150 min, taking 0.2 g of catalyst, and cyclohexanone/benzaldehyde (molar ratio 1:2). Results given in Table 4 show that Turkish perlite, TAP, and commercial NiO do not possess any catalytic activity for this reaction. In the case of NPC-10, a lower isolated yield (58%) is obtained due to the presence of fewer Bronsted acid sites on the catalytic

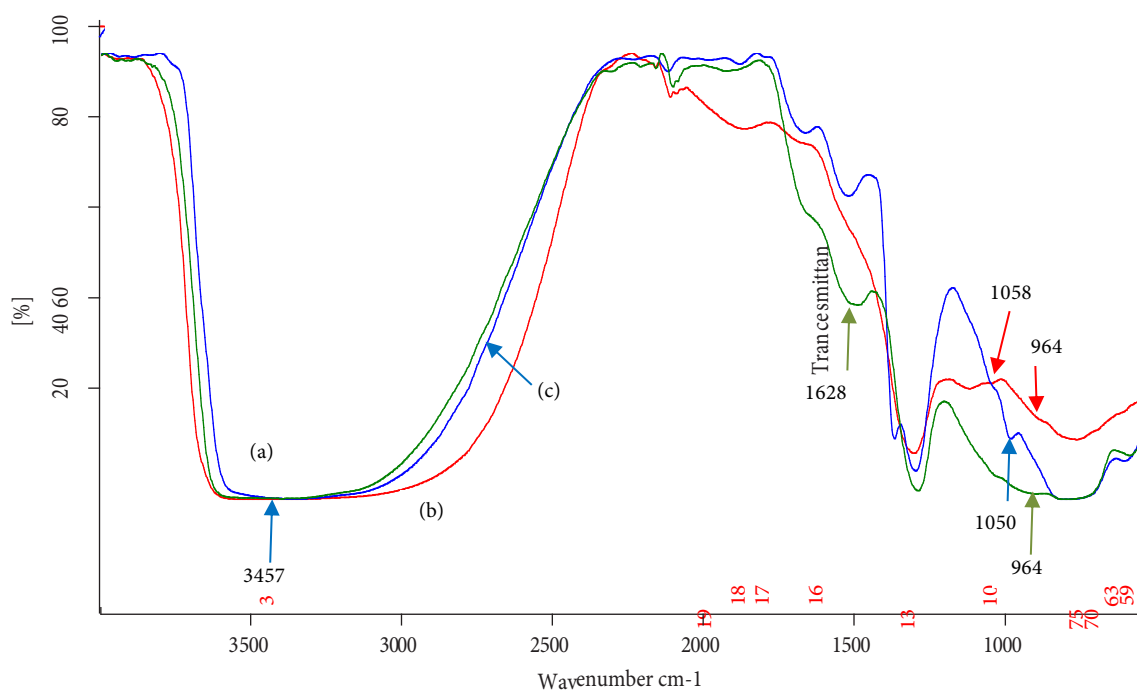


Figure 6. FT-IR spectra of (a) NPC-10, (b) NPC-15 and (c) NPC-50.

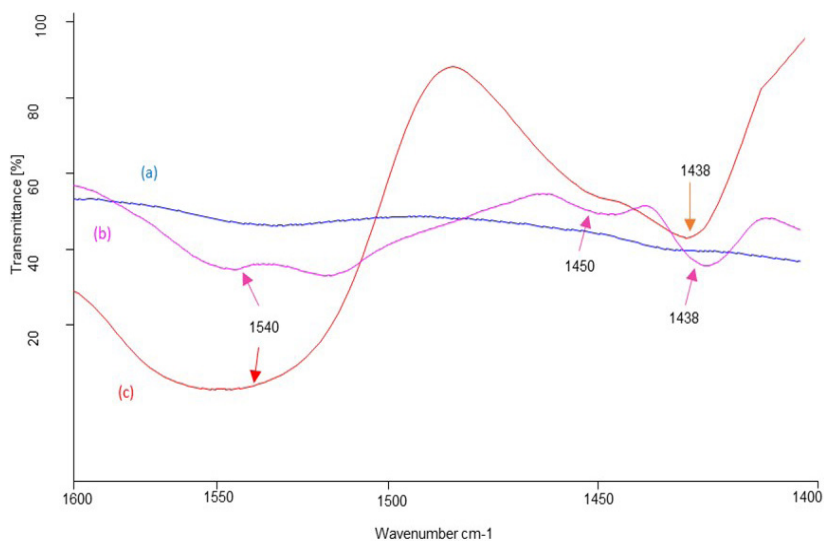


Figure 7. Pyridine adsorbed FT-IR spectra of (a) NPC-10, (b) NPC-15, and (c) NPC-50.

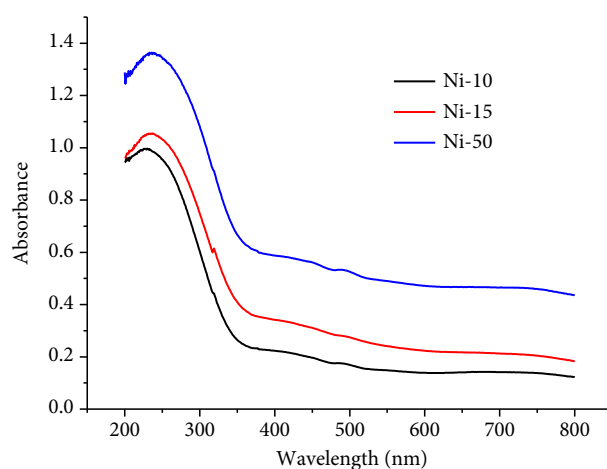


Figure 8. UV-Vis DRS spectra of NPC-10, 15, and 50.

surface, while, in the presence of NPC-15, the isolated yield % is highest due to significant increment of active catalytic sites. The isolated yield % is again decreased on using NPC-50 due to blockage of surface-active Bronsted acidic sites by bulk deposition of NiO crystallites.

As depicted from Table 5, NPC-15 gave a good isolated yield % of 2,6-bis(benzylidene)cyclohexanone in the first as well as in the last run with decent enough consecutive reaction runs when compared with some previously reported catalysts.

Based on these results, NPC-15 was chosen as the main catalyst for catalyzing a series of Claisen-Schmidt reactions (Table 6). In this series, the reactions of cyclohexanone and various aromatic aldehydes were studied for different periods at 110–140 °C taking 0.2 g of catalyst and cyclohexanone/aromatic aldehydes (molar ratio 1:2).

3.3. Proposed reaction mechanism

Based on results drawn from XRD, FT-IR, pyridine adsorbed FT-IR, UV-Vis DRS studies, models can be proposed for Turkish perlite, NPC-10, 15, and 50 catalysts (Scheme 3). They show the presence of Bronsted and Lewis acid sites on the surface of catalysts. The possible pathway for the production of 2,6-bis(substituted benzylidene)cyclohexanones by condensation of cyclohexanone and aromatic aldehydes catalyzed by NPC-15 is shown in Scheme 4. The surface Bronsted acidic sites of NPC-15 initiate the reaction by ketone protonation (protonation of carbonyl functional group) followed by abstraction of a proton from α -carbon of the ketone, and active enol intermediate form is produced. Thus, intermediate

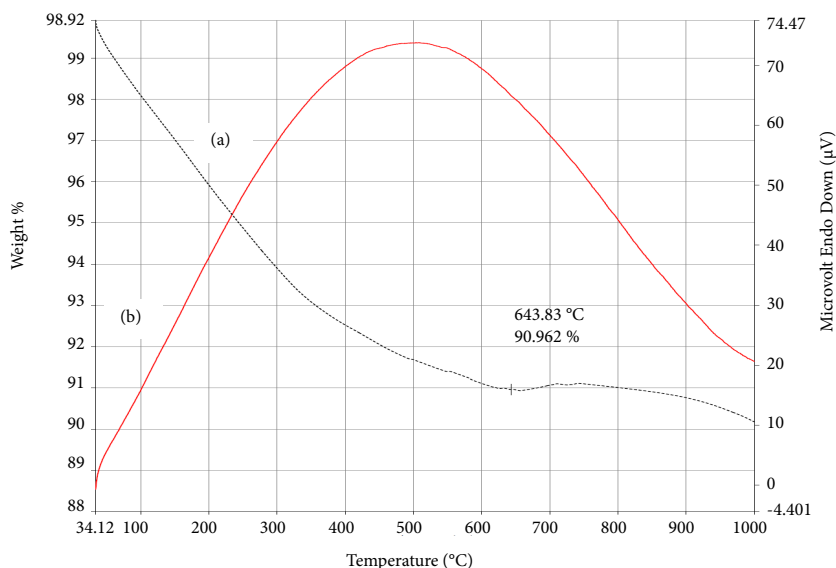


Figure 9. (a) TGA and (b) DSC curve of NPC-15.

Table 4. Catalytic activity of different catalysts for Claisen–Schmidt condensation reaction.

Catalysts	Isolated yield (%)
Turkish perlite	Nil
TAP	Nil
Commercial NiO	Nil
NPC-10	58
NPC-15	90
NPC-50	48

Reaction conditions: Time = 150 min; Temperature = 120 °C; molar ratio (cyclohexanone/benzaldehyde = 1:2); catalyst weight = 0.2g.

Table 5. Comparison of results using NPC-15 with some previously reported catalysts for Claisen–Schmidt condensation reaction between cyclohexanone and benzaldehyde.

Catalysts	Reusability of catalyst (No. of runs)	Isolated yield in 1st run (%)	Isolated yield in last run (%)
SiO ₂ -R-SO ₃ H ^a [71]	10	80	70
40% PW/N-SiO ₂ ^b [72]	04	98	86
Cs _{2.5} H _{0.5} PW ₁₂ O ₄₀ ^c [73]	05	74	~70
2-HEAA ^d [74]	-	93	-
NPC-15 ^e [This study]	06	90	83

Reaction conditions: ^aTime = 72 min; Temperature = 90 °C; molar ratio (cyclohexanone/benzaldehyde = 1:2); catalyst weight = 0.3 g.

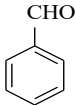
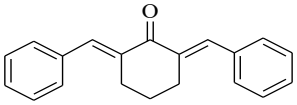
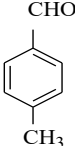
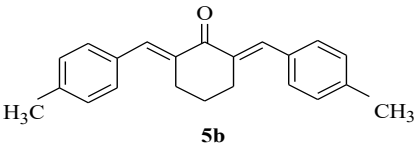
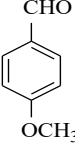
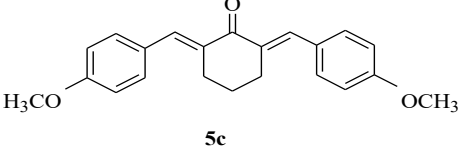
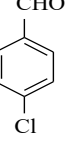
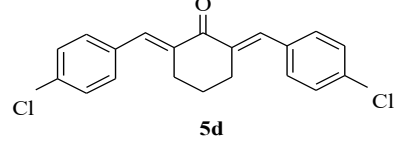
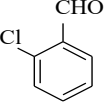
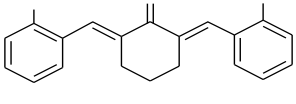
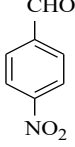
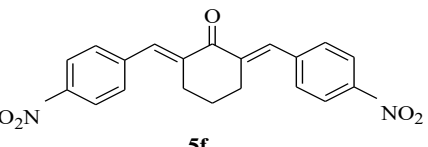
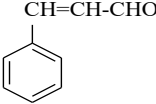
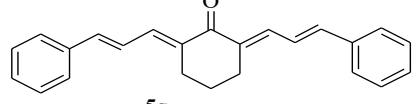
^bTime = 30 min; Temperature = Room temperature; molar ratio (cyclohexanone/benzaldehyde = 1:2); catalyst weight = 0.2 g.

^cTime = 10 min; Temperature = 50 °C; molar ratio (cyclohexanone/benzaldehyde = 1:2); catalyst weight = 8 mol%.

^dTime = 60 min; Temperature = 80 °C; molar ratio (cyclohexanone/benzaldehyde = 1:2); catalyst weight = 0.2 mmol.

^eTime = 150 min; Temperature = 120 °C; molar ratio (cyclohexanone/benzaldehyde = 1:2); catalyst weight = 0.2 g.

Table 6. NPC-15 catalyzed Claisen–Schmidt reaction between cyclohexanone and different aromatic aldehydes.

Entry	Aldehyde	Products ^b	Time (h)	Isolated yield (%)	M. pt. (°C)	
					Found	Reported
1		 5a	2.5	90	118	117 [75]
2		 5b	3	92	171	170 [76]
3		 5c	3	92	201	203-204 [77]
4		 5d	3	92	146	147-148 [76]
5		 5e	3.5	91	102	--
6		 5f	6	93	160	159 [77]
7		 5g	3	93	180	180 [77]

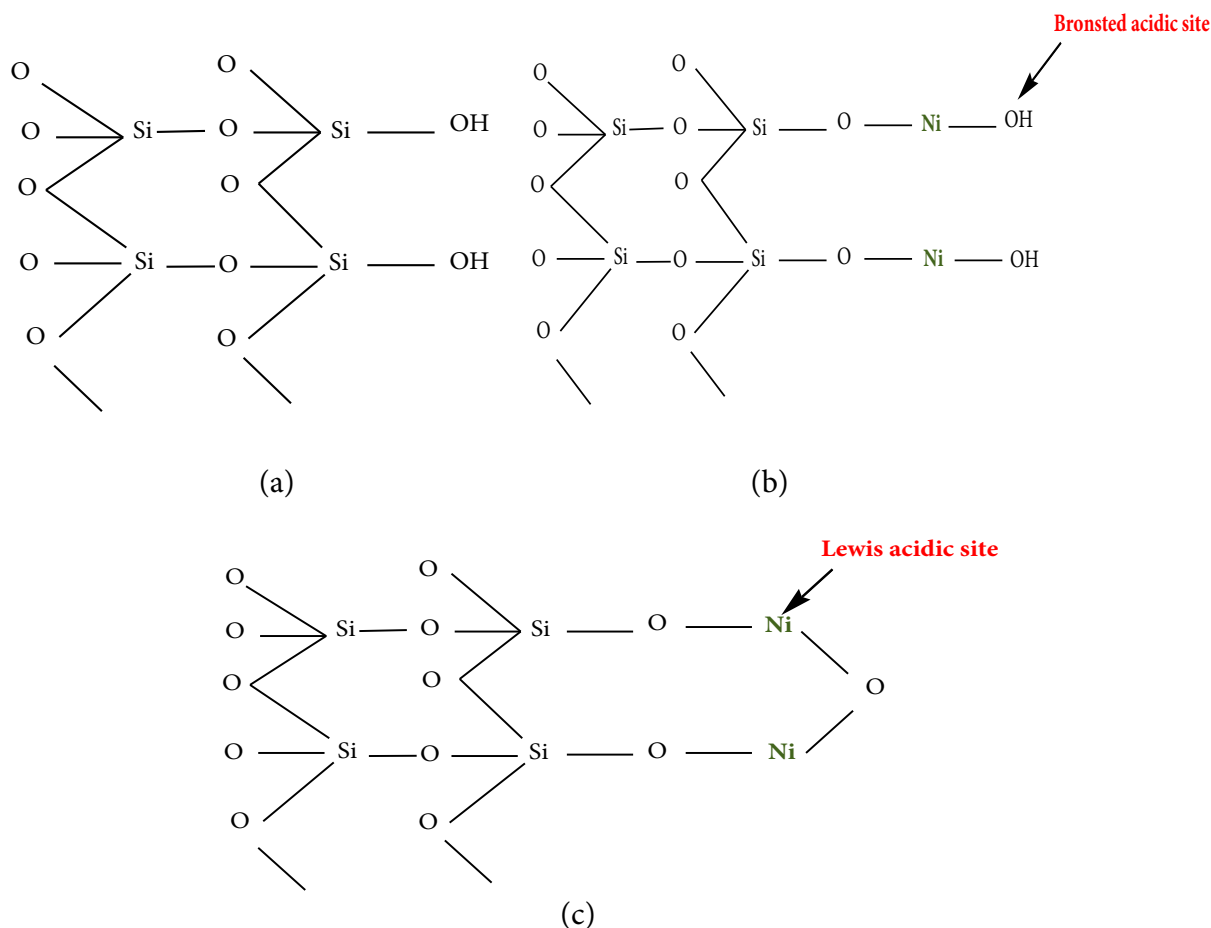
^a Reaction conditions: Temperature = 110–140 °C; molar ratio (cyclohexanone/aromatic aldehydes = 1:2); catalyst weight = 0.2 g.

^b Products (5a–5g) were characterized by melting point and spectral (IR and ¹H-NMR) data and compared with the literature.

form condenses with aromatic aldehydes via nucleophilic addition to form desired products and releases water as a side product.

3.4. Regeneration of catalyst

The spent catalyst was regenerated by doing simple filtration, washing with acetone, drying at 110 °C in an oven for 12 h, and finally by calcination at 450 °C in a muffle furnace for 1 h. Thus, obtained regenerated catalyst showed efficient catalytic activity up to consecutive 6 reaction cycles giving almost similar isolated yield % in the range of 90%–83%, indicating the presence of stabilized acidic sites in the regenerated catalyst. After the sixth reaction cycle, the yield % was decreased significantly, this may be due to blockage of acidic sites of the catalyst by the deposition of carbonaceous residues



Scheme 3. Proposed models of (a) Turkish perlite, (b) NPC-10, 15 and (c) NPC-50.

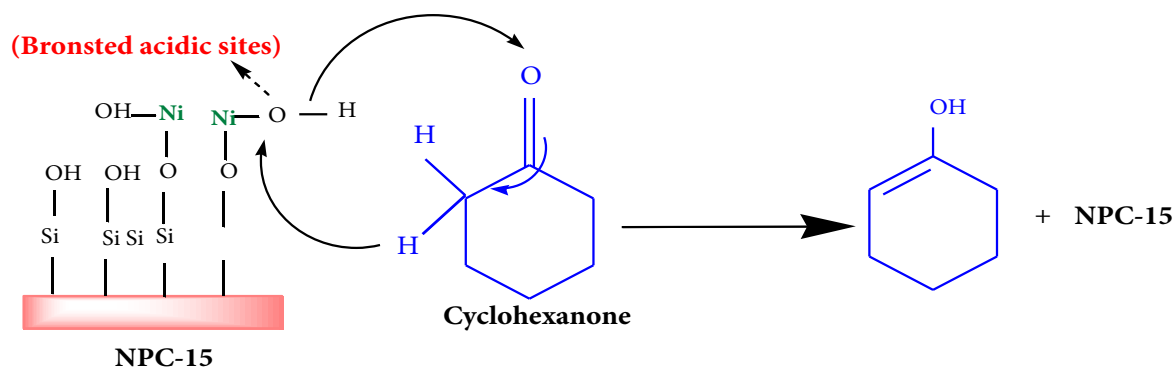
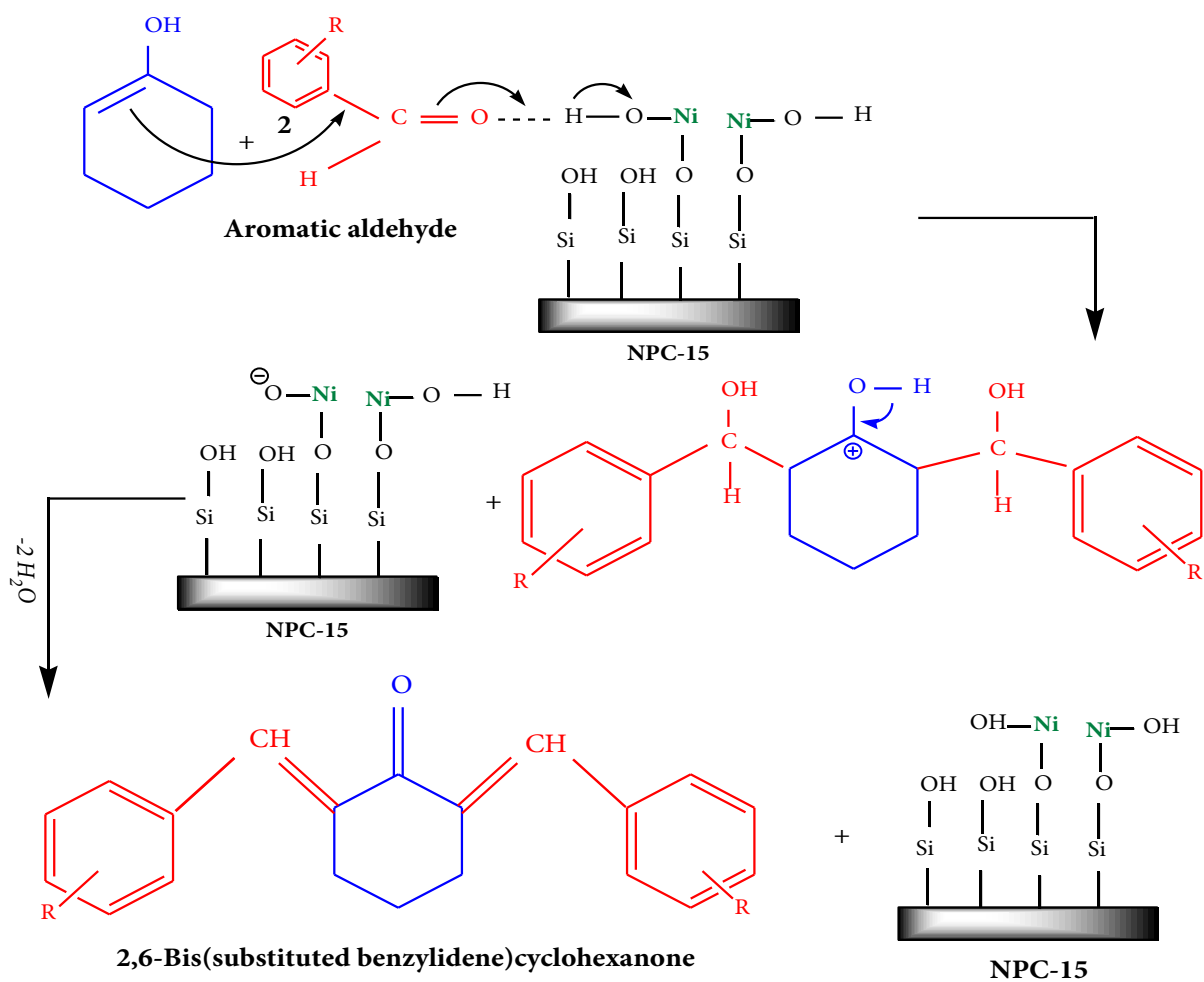
of organic reactants and products on the surface. The FT-IR spectrum (Figure 10) of regenerated NPC-15 regenerated after the sixth reaction cycle is similar to that of fresh NPC-15 demonstrating the stability of nickel oxide loading on Turkish perlite.

3.5. Product identification by $^1\text{H-NMR}$ (CDCl_3 , 500 MHz)

All the products synthesized by Claisen–Schmidt condensation reactions were identified by melting point analysis and $^1\text{H-NMR}$ spectroscopy. δ -values of all synthesized products are summarized in Table 7.

4. Conclusion

15 wt. % nickel oxide loaded on Turkish perlite (NPC-15) was proven to be an effective and competent solid acid catalyst, possessing significant Bronsted acidity to catalyze condensation reactions between cyclohexanone and aromatic aldehydes with high isolated yield (90%–93%) of desired products in one-pot, liquid phase, solvent-free reaction conditions. The catalyst was easily filtered, regenerated, and recycled several times with analogous efficiency, suggesting the stability of acidic sites of the catalyst during the reactions. The results of X-ray diffraction (XRD), Brunauer–Emmett–Teller (BET) surface area, pyridine adsorbed Fourier-transform infrared (FT-IR), etc. recommended that the optimum catalytic activity of NPC-15 was due to the presence of sufficient surface-active Brønsted acidic sites. While, at higher wt. % loading, NiO crystallites increased Lewis acidic sites and blocked the active Brønsted acidic sites, which ultimately decreased isolated yield % of desired products. XRD results depicted that, in NPC-15, nickel oxide particles were finely dispersed on the Turkish perlite surface in the amorphous phase. A fine dispersion of nickel oxide particles was also shown in scanning electron microscope (SEM) and transmission electron microscope (TEM) images of NPC-15. The novelty of this work is the utilization of abundant natural waste, Turkish perlite as solid support for the synthesis of highly efficient heterogeneous acid catalysts. This investigation also suggests that Turkish perlite could be an alternative to commercial silica for synthesizing novel solid acid catalysts, which can catalyze various industrially important reactions in a cost-effective manner.

Step- I**Step- II**

Scheme 4. Proposed mechanism of condensation of cyclohexanone and aromatic aldehydes over NPC-15.

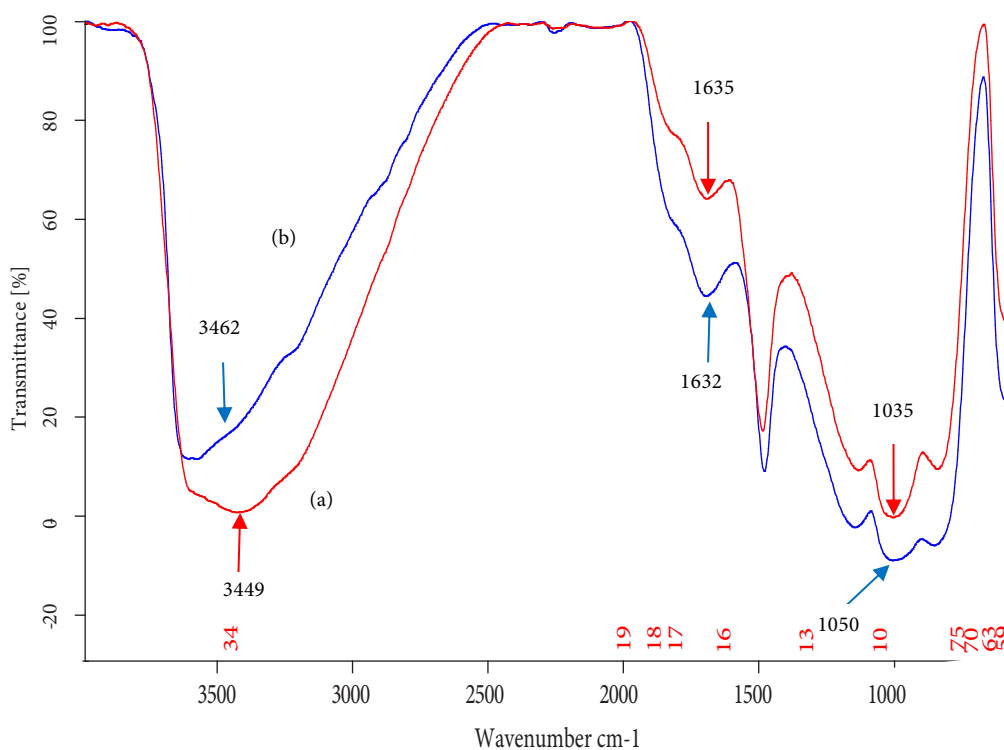


Figure 10. FT-IR spectra of (a) fresh NPC-15 and (b) regenerated NPC-15 after the sixth reaction cycle.

Table 7. Product Identification by $^1\text{H-NMR}$ (CDCl_3 , 500MHz).

Product name	Delta value (δ)
5a, 2,6-Dibenzylidenecyclohexanone	7.7 (s, 2H), 7.23-7.55 (m, 10H), 2.82-2.98 (m, 4H), 1.72-1.88 (m, 2H).
5b, 2,6-Di(p-methylbenzylidene)cyclohexanone	7.69 (s, 2H), 7.1-7.31 (m, 8H), 2.82-2.86 (t, 4H), 2.30 (s, 6H), 1.68-1.78 (p, 2H).
5c, 2,6-Di(p-methoxybenzylidene)cyclohexanone	7.66 (s, 2H), 6.88-7.26 (m, 8H), 3.68 (s, 6H), 2.72-2.84 (t, 4H), 1.68-1.8 (p, 2H).
5d, 2,6-Di(p-chlorobenzylidene)cyclohexanone	7.64 (s, 2H), 7.26-7.46 (m, 8H), 2.7-2.82 (t, 4H), 1.67-1.78 (p, 2H).
5e, 2,6-Di(o-chlorobenzylidene)cyclohexanone	7.81 (s, 2H), 7.16-7.28 (m, 8H), 2.67-2.76 (t, 4H), 1.68-1.8 (p, 2H).
5f, 2,6-Di(p-nitrobenzylidene)cyclohexanone	7.9 (s, 2H), 7.4-7.6 (m, 8H), 2.74-2.86 (t, 4H), 1.72-1.86 (p, 2H).
5g, 2,6-Dicinnamylidenecyclohexanone	6.78-7.21(m, 16H), 2.62-2.76 (t, 4H), 1.68-1.78 (p, 2H).

Acknowledgments

The authors are thankful to Dr. Mukul Gupta for XRD analysis, Dr. D.M. Phase, and Er. V.K. Ahiray for SEM, SEM-EDX analysis at UGC-DAE Consortium for Scientific Research, Indore, SAIF-Chandigarh for TEM analysis, and Dr. Sunil Sharma from IIT-Bombay for TGA analysis. The authors would like to acknowledge the financial support given by DST, New Delhi, India (Fly Ash Mission) and UGC, New Delhi India for the SRF scheme.

References

- Vekariya RH, Prajapati NP, Patel HD. Silica-supported polyphosphoric acid (PPA- SiO_2): An efficient and reusable heterogeneous catalyst for eco-friendly organic synthesis. *Synthetic communications* 2016; 46 (3): 197-219. doi: 10.1080/00397911.2015.1114633
- Lamba R, Kumar S, Sarkar S. Esterification of decanoic acid with methanol using Amberlyst 15: Reaction kinetics. *Chemical Engineering Communications* 2018; 205 (3): 281-294. doi: 10.1080/00986445.2017.1387540

3. Chandane VS, Rathod AP, Wasewar KL, Sonawane SS. Synthesis of cenosphere supported heterogeneous catalyst and its performance in esterification reaction. *Chemical Engineering Communications* 2018; 205 (2): 238-248. doi: 10.1080/00986445.2017.1384922
4. Hosseinzadeh Z, Ramazani A, Razzaghi-Asl N, Slepokura K, Lis T. Boric acid as an efficient and green catalyst for the synthesis of 2-amino-4,6-diaryl nicotinonitrile under microwave irradiation in solvent-free conditions. *Turkish Journal of Chemistry* 2019; 43: 464-474. doi:10.3906/kim-1807-101
5. Malpani SK, Rani A. A Greener route for synthesis of fly ash supported heterogeneous acid catalyst. *Materials Today: Proceedings* 2019; 9 (3): 551-559. doi: 10.1016/j.matpr.2018.10.375
6. Khatri C, Mishra MK, Rani A. Synthesis and characterization of fly ash supported sulfated zirconia catalyst for benzylation reactions. *Fuel Processing Technology* 2010; 91 (10): 1288-1295. doi: 10.1016/j.fuproc.2010.04.011
7. Khatri C, Jain D. Fly ash-supported cerium triflate as an active recyclable solid acid catalyst for Friedel–Crafts acylation reaction. *Fuel* 2010; 89 (12): 3853-3859. doi: 10.1016/j.fuel.2010.07.007
8. Rani A, Khatri C, Hada R. Fly ash supported scandium triflate as an active recyclable solid acid catalyst for Friedel-Crafts acylation reaction. *Fuel Processing Technology* 2013; 116: 366-373. doi: 10.1016/j.fuproc.2013.08.003
9. Malpani SK, Goyal D, Katara S, Rani A. Green, efficient and economical coal fly ash based phosphomolybdic acid catalysts: preparation, characterization and application. *Chemical Papers* 2021; 75: 3017-3034. doi: 10.1007/s11696-020-01501-x
10. Katara S, Kabra S, Goyal D, Hada R, Sharma A et al. Fly ash to solid base catalyst: synthesis, characterization and catalytic application. *Materials Today: Proceedings* 2021; 42 (2): 1409-1416. doi: 10.1016/j.matpr.2021.01.148
11. Vichaphund S, Aht-Ong D, Sricharoenchaikul V, Atong D. Characteristic of fly ash derived-zeolite and its catalytic performance for fast pyrolysis of *Jatropha* waste. *Environmental Technology* 2014; 35 (17): 2254-2261. doi: 10.1080/09593330.2014.900118
12. Wang Y, Zhang M, Ding X. Biodiesel production from soybean oil using modified calcium loaded on rice husk activated carbon as a low-cost basic catalyst. *Separation Science and Technology* 2018; 53 (5): 807-813. doi: 10.1080/01496395.2017.1374411
13. Tinh NT, Van NTT, Anh NP, Ha HKP, Tri N. CuO and CeO₂-doped catalytic material synthesized from red mud and rice husk ash for *p*-xylene deep oxidation. *Journal of Environmental Science and Health, Part A* 2019; 54 (4): 4352-4358. doi: 10.1080/10934529.2018.1551649
14. Vichaphund S, Sricharoenchaikul V, Atong D. Utilization of fly ash-derived HZSM-5: catalytic pyrolysis of *Jatropha* wastes in a fixed-bed reactor. *Environmental Technology* 2017; 38 (13-14): 1660-1672. doi: 10.1080/09593330.2016.1244567
15. Hwang H, Lee JH, Choi I, Choi JW. Comprehensive characterization of hydrothermal liquefaction products obtained from woody biomass under various alkali catalyst concentrations. *Environmental Technology* 2019; 40 (13): 1657-1667. doi: 10.1080/09593330.2018.1427799
16. Tsaousi G-M, Douni I, Paniais D. Experimental evaluation of efficient Si dissolution from perlite at low level activator's concentration. *Minerals* 2018; 8 (4): 160-167. doi: 10.3390/min8040160
17. Angelopoulos PM, Maliachova C, Papakonstantinou K, Taxiarchou M, Diplas S. Structural and physical characteristics of fine perlite expanded with a novel method in a vertical electric furnace. *Mineral Processing and Extractive Metallurgy* 2016; 125: 71-80. doi: 10.1080/03719553.2016.1156244
18. Bastani D, Safekordi AA, Alihosseini A, Taghikhani V. Study of oil sorption by expanded perlite at 298.15 K. *Separation and Purification Technology* 2006; 52: 295-300. doi: 10.1016/j.seppur.2006.05.004
19. Dogan M, Alkan M. Adsorption kinetics of methyl violet onto perlite. *Chemosphere* 2003; 50 (4): 517-528. doi: 10.1016/S0045-6535(02)00629-X
20. Rashad AM. A synopsis about perlite as building material – A best practice guide for civil engineer. *Construction and Building Materials* 2016; 121: 338-353. doi: 10.1016/j.conbuildmat.2016.06.001
21. Mostaedi MT, Ghassabzadeh H, Maragheh MG, Ahmadi SJ, Taheri H. Removal of Cadmium and Nickel from aqueous solution using expanded perlite. *Brazilian Journal of Chemical Engineering* 2010; 27 (2): 299-308. doi: 10.1590/S0104-66322010000200008
22. Silber A, Bar-Yosef B, Levkovitch I, Kautzky L, Minz D. Kinetics and mechanisms of pH-dependent Mn (II) reactions in plant-growth medium. *Soil Biology Biochemistry* 2008; 40: 2787-2795. doi: 10.1016/j.soilbio.2008.07.026
23. Zhang S, Li H, Yang Z. Synthesis, structural characterization and evaluation of a novel floating metal-free photocatalyst based on g-C₃N₄ grafted expanded perlite for the degradation of dyes. *Materials Technology* 2018; 33 (1): 1-9. doi: 10.1080/10667857.2017.1367148
24. Balat M. Diesel-like fuel obtained by catalytic pyrolysis of waste engine oil. *Energy, Exploration and Exploitation* 2008; 26 (3): 197-208. doi: 10.1260/014459808786933735
25. Kolvari E, Koukabi N, Hosseini MM, Khandani Z. Perlite: an inexpensive natural support for heterogenization of HBF₄. *RSC Advances*, 2015; 5: 36828-36836. doi: 10.1039/c5ra03229f
26. Radonjic V, Krstic J, Loncarevic D, Jovanovic D, Vukelic N et al. Perlite as a potential support for nickel catalyst in the process of sunflower oil hydrogenation. *Russian Journal of Physical Chemistry A* 2015; 89 (13): 2359-2366. doi: 10.1134/S0036024415130294

27. Brindha K, Amutha P, Krishnakumar B, Sobral AJFN. BiCl₃-modified perlite as an effective catalyst for selective organic transformations: a green protocol. *Research on Chemical Intermediates* 2019; 45: 4367-4381. doi: 10.1007/s11164-019-03836-x
28. Rostami-Vartooni A, Nasrollahzadeh M, Alizadeh M. Green synthesis of perlite supported silver nanoparticles using *Hamamelis virginiana* leaf extract and investigation of its catalytic activity for the reduction of 4-nitrophenol and Congo red. *Journal of Alloys and Compounds* 2016; 680: 309-314. doi: 10.1016/j.jallcom.2016.04.008
29. Nasrollahzadeh M, Sajadi SM, Rostami-Vartooni A, Bagherzadeh M, Safari R. Immobilization of copper nanoparticles on perlite: Green synthesis, characterization and catalytic activity on aqueous reduction of 4-nitrophenol. *Journal of Molecular Catalysis A: Chemical* 2015; 400: 22-30. doi: 10.1016/j.molcata.2015.01.032
30. Kolvari E, Koukabi N, Hosseini MM. Perlite: A cheap natural support for immobilization of sulfonic acid as a heterogeneous solid acid catalyst for the heterocyclic multicomponent reaction. *Journal of Molecular Catalysis A: Chemical* 2015; 397: 68-75. doi: 10.1016/j.molcata.2014.10.026
31. Ermakova MA, Ermakov DY. High-loaded nickel-silica catalysts for hydrogenation, prepared by sol-gel Route: structure and catalytic behavior. *Applied Catalysis A: General* 2003; 245: 277-288. doi: 10.1016/S0926-860X(02)00648-8
32. Achouri IE, Abatzoglou N, Lefebvre CF, Braidy N. Diesel steam reforming: Comparison of two nickel aluminate catalysts prepared by wet-impregnation and co-precipitation. *Catalysis Today* 2013; 207: 13-20. doi: 10.1016/j.cattod.2012.09.017
33. Rodríguez JL, Valenzuela MA, Tiznado H, Poznyak T, Chairez I et al. A comparative study of alumina-supported Ni catalysts prepared by photodeposition and impregnation methods on the catalytic ozonation of 2,4-dichlorophenoxyacetic acid. *Journal of Nanoparticle Research* 2017; 19 (54): 1-11. doi: 10.1007/s11051-017-3766-1
34. Frontera P, Macario A, Aloise A, Crea F, Antonucci PL et al. Catalytic dry-reforming on Ni-zeolite supported catalyst. *Catalysis Today* 2012; 179 (1): 52-60. doi: 10.1016/j.cattod.2011.07.039
35. Zhang L, Wen X, Kong T, Zhang L, Gao L et al. Preparation and mechanism research of Ni-Co supported catalyst on hydrogen production from coal pyrolysis. *Scientific Reports* 2019; 9: 1-13. doi: 10.1038/s41598-019-44271-7
36. Solsona B, Concepcion P, Lopez Nieto JM, Dejoz A, Cecilia JA et al. Nickel oxide supported on porous clay heterostructures as selective catalysts for the oxidative dehydrogenation of ethane. *Catalysis Science and Technology* 2016; 6: 3419-3429. doi: 10.1039/C5CY01811K
37. Hada R, Goyal D, Yadav VS, Siddiqui N, Rani A. Synthesis of NiO nanoparticles loaded fly ash catalyst via microwave assisted solution combustion method and application in hydrogen peroxide decomposition. *Materials Today: Proceedings* 2020; 28 (1): 119-123. doi: 10.1016/j.matpr.2020.01.411
38. Chistyakov AV, Zharova PA, Nikolaev SA, Tsodikov MV. Direct Au-Ni/Al₂O₃ catalysed cross-condensation of ethanol with isopropanol into pentanol-2. *Catalysis Today* 2017; 279 (1): 124-132. doi: 10.1016/j.cattod.2016.06.016
39. Hermida L, Abdullah AZ, Mohamed AR. Synthesis and characterization of mesostructured cellular foam (MCF) silica loaded with nickel nanoparticles as a novel catalyst. *Materials Sciences and Applications* 2013; 4: 52-62. doi: 10.4236/msa.2013.41007
40. Dimmock JR, Hamon NW, Hindmarsh KW, Sellar AP, Turner WA et al. Evaluation of 2-benzylidenecyclohexanones and 2,6-bis(benzylidene)cyclohexanones for antitumor and cytotoxic activity and as inhibitors of mitochondrial function in yeast: Metabolism studies of (E)-2-benzylidenecyclohexanone. *Journal of Pharmaceutical Sciences* 1976; 65 (4): 538-543. doi: 10.1002/jps.2600650415
41. Kang LQ, Song GH, Wang JY, Wei BG. Synthesis of α, α' -Bis(Substituted Benzylidene)cycloalkanes catalyzed by amino-functionalized ionic liquid. *Journal of The Chinese Chemical Society* 2008; 55: 1125-1128. doi: 10.1002/jccs.200800165
42. Rahman MAFM, Ali R, Jahng Y, Kadi AA. A facile solvent free Claisen-Schmidt Reaction: Synthesis of α, α' -Bis-(Substituted-benzylidene)cycloalkanes and α, α' -Bis-(Substituted-alkylidene)cycloalkanes. *Molecules* 2012; 17 (1): 571-583. doi: 10.3390/molecules17010571
43. Tsay MT, Chang FW. Characterization of rice husk ash-supported nickel catalysts prepared by ion exchange. *Applied Catalysis A: General* 2000; 203: 15-22. doi: 10.1016/S0926-860X(00)00464-6
44. Merabti R, Bachari K, Halliche D, Rassoul Z, Saadi A. Synthesis and characterization of activated carbon-supported copper or nickel and their catalytic behavior towards benzaldehyde hydrogenation. *Reaction Kinetics, Mechanisms and Catalysis* 2010; 101: 195-208. doi: 10.1007/s11144-010-0215-x
45. Acosta D, Martinez J, Carrera C, Erdmann E, Gonzo E et al. New material as support for nickel boride catalyst. *Latin American Applied Research* 2006; 36: 317-320.
46. Zhao A, Ying W, Zhang H, Ma H, Fang D. Ni-Al₂O₃ catalysts prepared by solution combustion method for syngas methanation. *Catalysis Communications* 2012; 17: 34-38. doi: 10.1016/j.catcom.2011.10.010
47. Zangouei M, Moghaddam AZ, Arasteh M. The influence of nickel loading on reducibility of NiO/Al₂O₃ catalysts synthesized by sol-gel method. *Chemical Engineering Research Bulletin* 2010; 14: 97-102. doi: 10.3329/cerb.v14i2.5052
48. Kalapathy U, Proctor A, Shultz J. A simple method for production of pure silica from rice husk ash. *Bioresource Technology* 2000; 73 (3): 257-262. doi: 10.1016/S0960-8524(99)00127-3

49. Jain D, Khatri C, Rani A. Synthesis and characterization of novel solid base catalyst from fly ash. *Fuel* 2011; 90: 2083-2088. doi: 10.1016/j.fuel.2010.09.025
50. Javed SH, Naveed S, Feroze N, Zafar M, Shafaq M. Crystal and Amorphous Silica from KMnO_4 Treated and Untreated Rice Husk. *Journal of Quality and Technology Management* 2010; 6 (1): 81-90. Corpus ID: 173171822
51. Martinez JR, Palomares-Sanchez S, Ortega-Zarzosa G, Ruiz F, Chumakov Y. Rietveld refinement of amorphous SiO_2 prepared via sol-gel method. *Materials Letters* 2006; 60: 3526-3529. doi: 10.1016/j.matlet.2006.03.044
52. Prakasham RS, Devi GS, Rao CS, Sivakumar VSS, Sathish T et al. Nickel impregnated silica nanoparticle synthesis and their evaluation for biocatalyst immobilization. *Applied Biochemistry Biotechnology* 2010; 160: 1888-1895. doi: 10.1007/s12010-009-8726-5
53. Gamman JJ, Millar GJ, Rose G, Drennan J. Characterization of SiO_2 -supported nickel catalysts for carbon dioxide reforming of methane. *Journal of the Chemical Society Faraday Transactions* 1998; 94 (5): 701-710. doi: 10.1039/A706730E
54. He M, Chernov AI, Obratsova ED, Sainio J, Rikkinen E et al. Low temperature growth of SWNTs on a nickel catalyst by thermal chemical vapor deposition. *Nano Research* 2011; 4 (4): 334-342. doi: 10.1007/s12274-010-0088-3
55. Kaufhold S, Reese A, Schwiebacher W, Dohrmann R, Grathoff GH et al. Porosity and distribution of water in perlite from the island of Milos, Greece. *SpringerPlus* 2014; 3 (598): 1-10. doi: 10.1186/2193-1801-3-598
56. Saufi H, Alouani ME, Alehyen S, Achouri ME, Aride J et al. Photocatalytic degradation of methylene blue from aqueous medium onto perlite-based geopolymer. *International Journal of Chemical Engineering* 2020; 2020: 1-7. doi: 10.1155/2020/9498349
57. Celik AG, Kilic M, Cakal GO. Expanded perlite aggregate characterization for use as a lightweight construction raw material. *Physicochemical Problems of Mineral Processing* 2013; 49 (2): 689-700. doi: 10.5277/ppmp130227
58. Fazaeli R, Aliyan H, Foroushani SP, Mohagheghian Z. PW_{12} -APTES@MCF: effective nanosized mesoporous composites for the oxidation of benzyl alcohols. *Turkish Journal of Chemistry* 2014; 38: 372-380. doi:10.3906/kim-1212-40
59. Jain D, Mishra M, Rani A. Synthesis and characterization of novel aminopropylated fly ash catalyst and its beneficial application in base catalyzed Knoevenagel condensation reaction. *Fuel Processing Technology* 2012; 95: 119-126. doi: 10.1016/j.fuproc.2011.12.005
60. Tahiri N, Khouchaf L, Elaatmani M, Louarn G, Zegzouti A et al. Study of the thermal treatment of SiO_2 aggregate. *IOP Conference Series: Materials Science and Engineering* 2014; 62 (012002): 1-8. doi:10.1088/1757-899X/62/1/012002
61. Saikia BJ, Parthasarathy G. Fourier transform infrared spectroscopic characterization of kaolinite from Assam and Meghalaya, Northeastern India. *Journal of Modern Physics* 2010; 1 (4): 206-210. doi: 10.4236/jmp.2010.1.4031
62. Huang X, Yin G, Feng G. Organic modification of montmorillonite and effect of catalytic selectivity on the dimerization of unsaturated fatty acid. *Turkish Journal of Chemistry* 2018; 42: 50-62. doi:10.3906/kim-1704-61
63. Ermakova MA, Ermakov DY. High-loaded nickel-silica catalysts for hydrogenation, prepared by sol-gel Route: structure and catalytic behaviour. *Applied Catalysis A: General* 2003; 245: 277-288. doi: 10.1016/S0926-860X(02)00648-8
64. Wu ZY, Wang YM, Huang WW, Yang J, Wang HJ et al. Formation of cubic Ia3d silicas and metal oxide-loaded silicas using a triblock copolymer $(\text{EO}_{20}\text{PO}_{70}\text{EO}_{20})$ -acetate mixture as structure director in aqueous solution. *Chemistry of Materials* 2007; 19 (7): 1613-1625. doi: 10.1021/cm0623615
65. Reddy CR, Bhat YS, Nagendrappa G, Jai Prakash BS. Brønsted and Lewis acidity of modified montmorillonite clay catalysts determined by FT-IR spectroscopy. *Catalysis Today* 2009; 141 (1-2): 157-160. doi: 10.1016/j.cattod.2008.04.004
66. Musthofa M, Karim AH, Fadzilliah NA, Hazirah N, Annuar NHR et al. Determination of Lewis and Brønsted acid sites by gas flow-injection technique. *Malaysian Journal of Fundamental and Applied Sciences* 2010; 6 (2): 127-131. doi: 10.11113/mjfas.v6n2.195
67. Wang Z, Navarette J. Keggin structure and surface acidity of 12-Phosphotungstic acid grafted Zr-MCM-48 mesoporous molecular sieves. *World Journal of Nano Science and Engineering* 2012; 2 (3): 134-141. doi: 10.4236/wjnse.2012.23017
68. Liu D, Quek XY, Cheo WNE, Lau R, Borgna A et al. MCM-41 supported nickel based bimetallic catalysts with superior stability during carbon dioxide reforming of methane: Effect of strong metal-support interaction. *Journal of Catalysis* 2009; 266 (2): 380-390. doi: 10.1016/j.jcat.2009.07.004
69. Lin C, Shaheen A, Muhtaseb A, Ritter JA. Thermal Treatment of Sol-Gel Derived Nickel Oxide Xerogels. *Journal of Sol-Gel Science and Technology* 2003; 28: 133-141. doi: 10.1023/A:1025653607374
70. Savva PG, Goundani K, Vakros J, Bourikas K, Fountzoula C et al. Benzene hydrogenation over $\text{Ni}/\text{Al}_2\text{O}_3$ catalysts prepared by conventional and sol-gel techniques. *Applied Catalysis B: Environmental* 2008; 79 (3): 199-207. doi: 10.1016/j.apcatb.2007.10.023
71. Habibi A, Sheikhhosseini E, Bigdeli M, Balalaie S, Farrokhi E. Solvent Free Synthesis of α , β -Bis(substituted-benzylidene)cycloalkanones Using Covalently Anchored Sulfonic Acid on Silica Gel (SiO_2 -R-SO₃H) as an Efficient and Reusable Heterogeneous Catalyst. *International Journal of Organic Chemistry* 2011; 1 (4): 143-147. doi: 10.4236/ijoc.2011.1.4021

72. Rafiee E, Shahebrahimi S. Nano silica with high surface area from rice husk as a support for 12-Tungstophosphoric acid: an efficient nano catalyst in some organic reactions. *Chinese Journal of Catalysis* 2012; 33 (8): 1326-1333. doi: 10.1016/S1872-2067(11)60420-8
73. Rafiee E, Rahimi F. A green approach to the synthesis of chalcones via Claisen-Schmidt condensation reaction using cesium salts of 12-tungstophosphoric acid as a reusable nanocatalyst. *Monatshefte für Chemie* 2013; 144: 361-367. doi: 10.1007/s00706-012-0814-5
74. Kang LQ, Cai YQ, Wang H, Li LH. Solvent-free catalytic preparation of 2,6-dibenzylidenecycloalkanones using 2-hydroxyethylammonium acetate ionic liquid as catalyst. *Monatshefte für Chemie* 2014; 145: 337-340. doi: 10.1007/s00706-013-1082-8